Electronic Supplementary Information

Copper-bipyridine grid frameworks incorporated with redox-active tetrathiafulvalene: structures and supercapacitance

Zi-Yao Zhou,[a] Chen-Yi Ge,[a] Miao Jiang,[a] Jin-Le Hou,[b] Qin-Yu Zhu,*[a] and Jie Dai*[a]

[a] College of Chemistry, Chemical Engineering and Materials Science, Soochow University, Suzhou 215123, People's Republic of China.

[b] School of Chemistry and Chemical Engineering, Liaocheng University, Liaocheng, 252059, People's Republic of China.

Qin-Yu Zhu, E-mail: zhuqinyu@suda.edu.cn

Jie Dai, E-mail: daijie@suda.edu.cn

1. EXPERIMENTAL

2. FIGURES

Fig. S1. The experimental powder XRD patterns and the simulated patterns from the crystal data of compounds **1**–**3**.

Fig. S2. IR spectra of Na_2L and compounds **1**–**3**.

Fig. S3. (a)–(c) Asymmetric unit of **1**–**3**.

Fig. S4. The plane of HL in compound **1**.

Fig. S5. Structure of 2D (4,4) grid topology of **2**, showing the different conformations of the bpe ligands in *b* and *c* directions.

Fig. S6. The plane of HL in column 1 (a) and column 2 (b) of compound **2**.

Fig. S7. The 2D plane of **3** viewed along two different sides.

Fig. S8. The plane of HL in compound **3**.

Fig. S9. Curves of the peak currents vs the square roots of scan rates of **2** for CV measurements.

Fig. S10. (a) CV curves of **1** at different scan rates. (b) Curves of the peak currents vs the square roots of scan rates of **1**. (c) GCD curves of **1** at different current intensities.

Fig. S11. (a) CV curves of **3** at different scan rates. (b) Curves of the peak currents vs the square roots of scan rates of **3**. (c) GCD curves of **3** at different current intensities.

3. TABLES

Table S1. Crystal data and structural refinement parameters for compounds **1**–**3**.

4. EQUATIONS

1. EXPERIMENTAL

General Remarks.

The sodium salt of dimethylthio-tetrathiafulvalene–bicarboxylate (Na$_2$L) was prepared according to the literature.[1,2] All analytically pure reagents were purchased commercially and used without further purification. Elemental analyses (C, H, and N) were performed using a VARIDEL III elemental analyzer. Solid-state room-temperature optical diffuse reflectance spectra of the microcrystal samples were obtained with a Shimadzu UV-2600 spectrophotometer using BaSO$_4$ as a standard reference. Powder X-ray diffraction (PXRD) data were obtained using a D/MAX-3C X-ray diffraction meter with CuKα (λ = 1.5406 Å) radiation. Cyclic voltammetry (CV) experiments were performed on a CHI660 electrochemistry workstation in a three-electrode system with a Pt plate working electrode, a saturated calomel electrode (SCE) as reference electrode, and Pt wire as the auxiliary electrode. Electron spin resonance (ESR) spectra were carried out at 120 K and obtained using a Bruker ER-420 spectrometer with a 100 kHz magnetic field in X band.

X-ray Crystallographic Study.

The crystal data of **1**–**3** were collected using a Bruker APEX-II CCD diffractometer equipped with graphite monochromated Mo Kα (λ = 0.71075 Å) radiation were used to carry out the measurements at low temperatures. An absorption correction (multiscan) was applied for all these compounds. The structures were solved by direct methods using SHELXS-16 program and the refinements were performed against F^2 using SHELXL-16.[3,4] All the nonhydrogen atoms are refined anisotropically. The

hydrogen atoms are positioned with idealized geometry and refined with fixed isotropic displacement parameters. Detailed crystal data and structural refinement parameters are listed in Table S1 in the Supporting Information.

Electrode Preparation and Photocurrent Measurement.

The photoelectrodes of the compounds were prepared by powder coating method. As a typical procedure, the crystals of compounds (0.005 mmol) were ground and pressed uniformly on the ITO glass (1.0×1.0 cm, 8 Ω/□). A 150 W high–pressure xenon lamp, located 20 cm away from the surface of the ITO electrode, was employed as a full-wavelength light source. The photocurrent experiments were performed at room temperature on a CHI660E electrochemistry workstation in a three-electrode system, with the sample coated ITO glass as the working electrode mounted on the window with an area of 0.50 cm^2, a Pt wire as auxiliary electrode and a saturated calomel electrode (SCE) as reference electrode. The supporting electrolyte solution was a 0.1 mol·L^{-1} sodium sulfate aqueous solution. The lamp was kept on continuously, and a manual shutter was used to block exposure of the sample to the light. The sample was typically irradiated at intervals of 20 s.

Fabrication of the working electrodes and electrochemical measurements.

The working electrodes were obtained with the following procedure. The compounds as active materials, acetylene black, and a poly(vinylene fluoride) (PVDF) emulsion, were mixed in ethanol at a weight ratio of 75 : 15 : 10, and dispersed by ultrasonic treatment for 10 min. The slurry was coated on a nickel foam (1.0 × 1.0 cm^2) current collector and then pressed and dried under vacuum at 60 °C for 12 h. The

mass of the active loading on the nickel foam was ~3 mg. The electrochemical properties of the active material were tested using a CHI660E electrochemical workstation by a conventional three-electrode system with a calomel reference electrode and a platinum counter electrode. The average specific capacitances of the electrodes were calculated based on the CV curves and the discharge curves, respectively. All of the electrochemical measurements were performed in a 6.0 M KOH solution at room temperature.
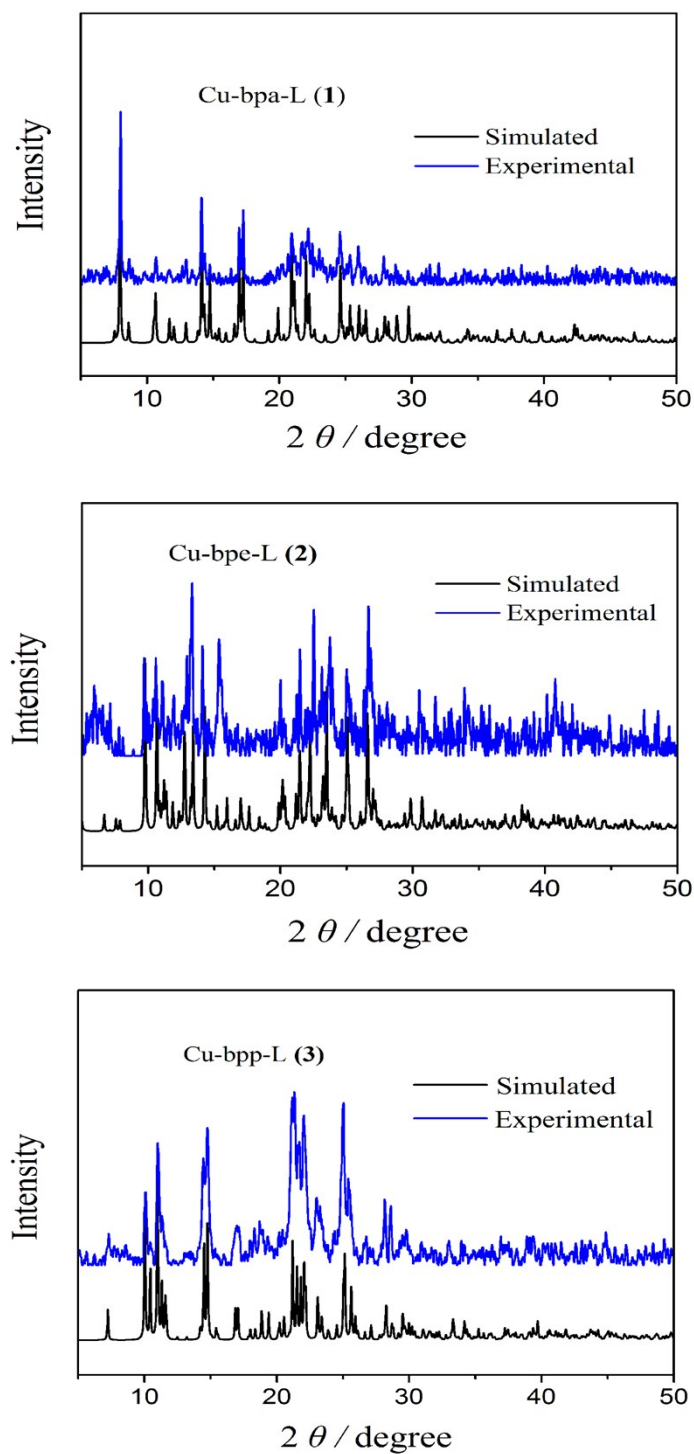
2. FIGURES

Fig. S1. The experimental powder XRD patterns and the simulated patterns from the crystal data of compounds **1**–**3**.
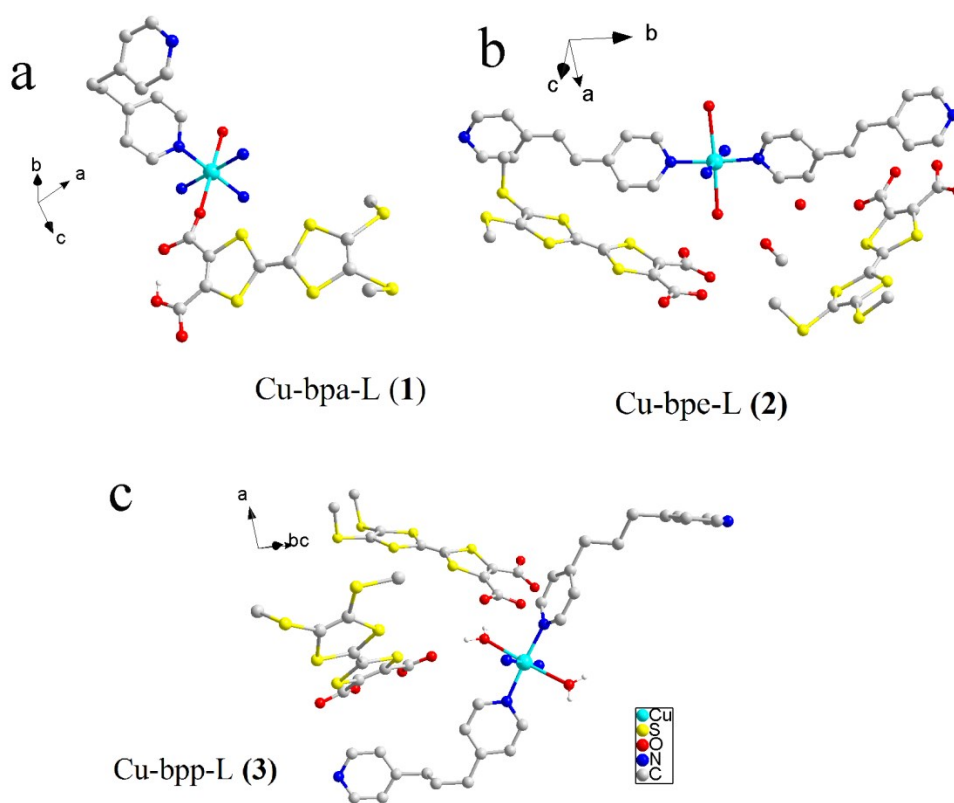
Fig. S2. IR spectra of Na$_2$L and compounds **1**–**3**.

Cu-bpa-L (**1**)

Cu-bpe-L (**2**)

Cu-bpp-L (**3**)
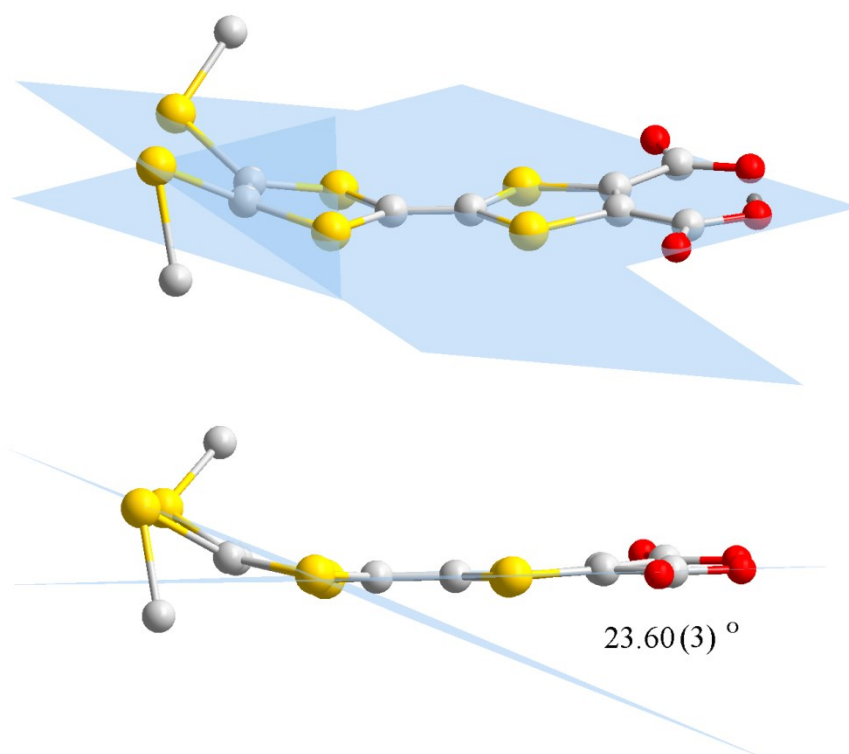
Fig. S3. (a)–(c) Asymmetric unit of **1**–**3**.

Fig. S4. The plane of HL in compound **1**.

23.60(3) °

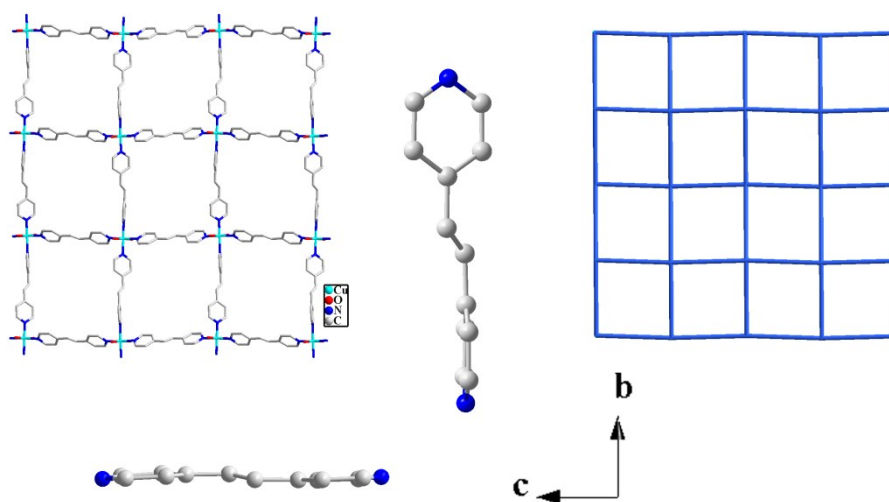**Fig. S5.** Structure of 2D (4,4) grid topology of **2**, showing the different conformations of the bpe ligands in *b* and *c* directions.
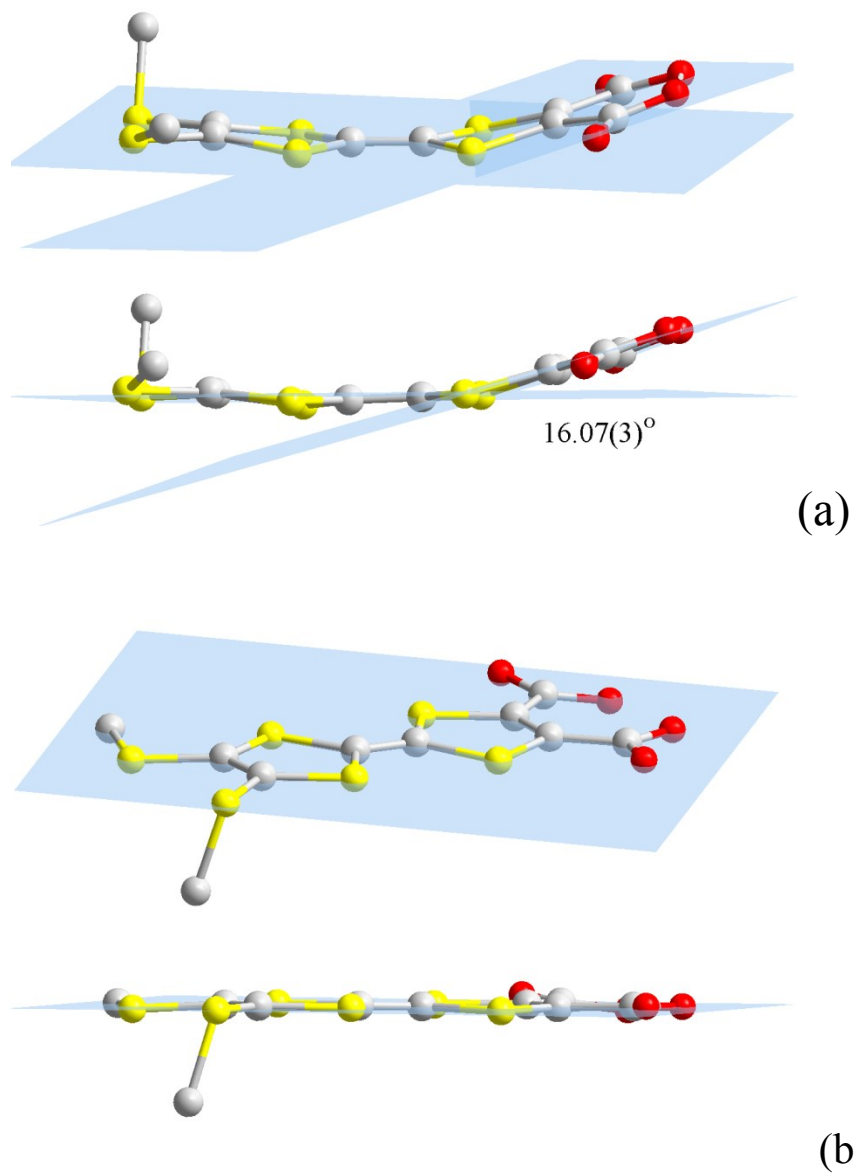
16.07(3)°

(a)

(b)

Fig. S6. The plane of HL in column 1 (a) and column 2 (b) of compound **2**.
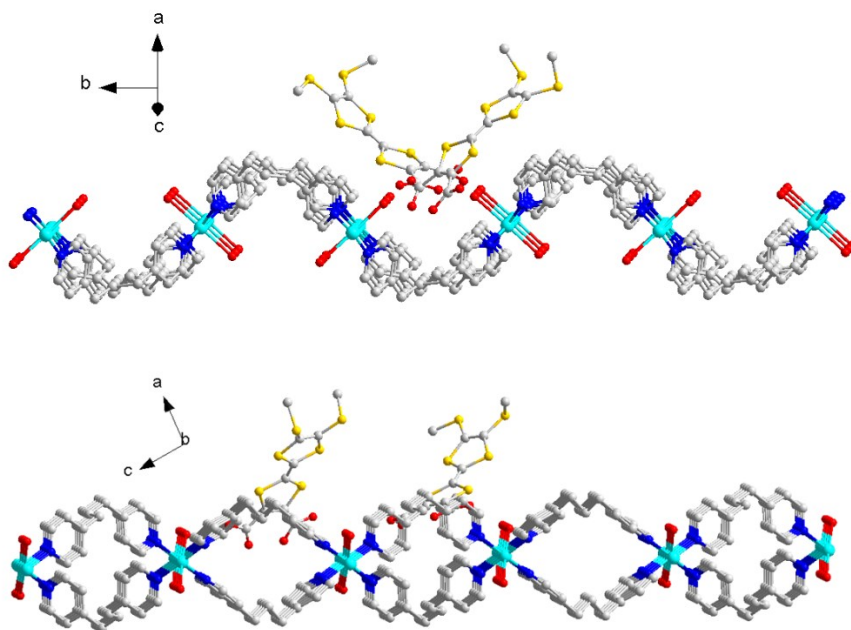
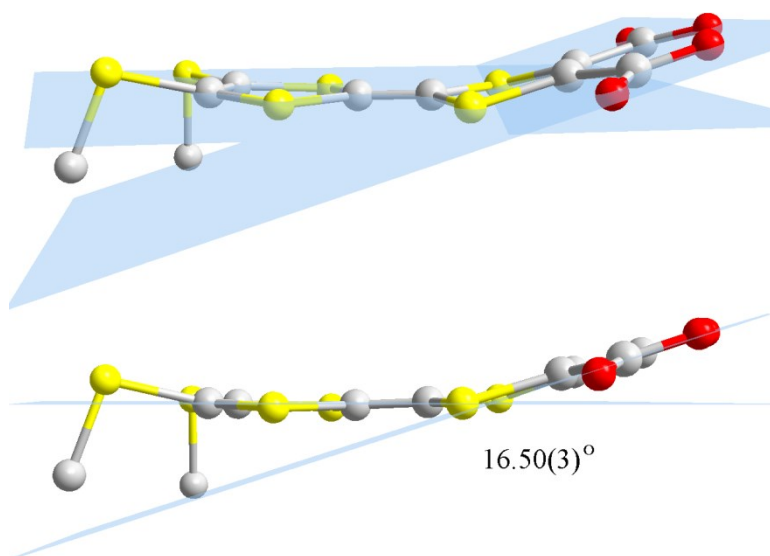**Fig. S7.** The 2D plane of **3** viewed along two different sides.

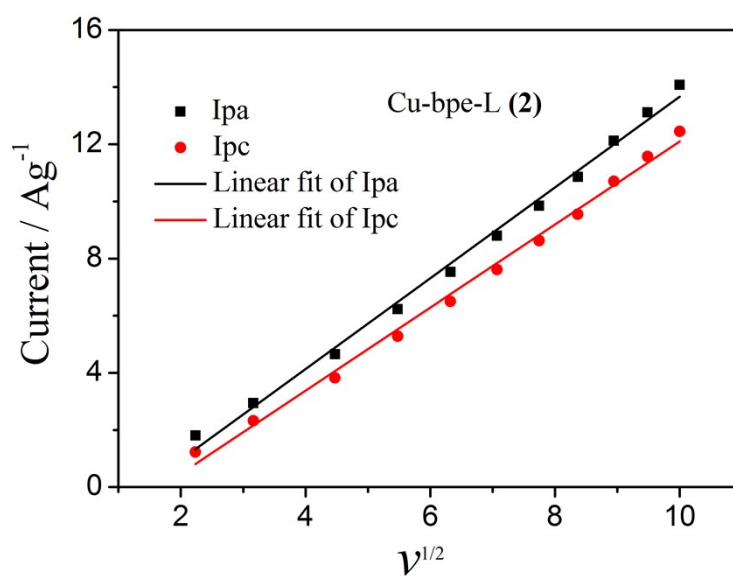**Fig. S8.** The plane of HL in compound **3**.

16.50(3)°

Fig. S9. Curves of the peak currents vs the square roots of scan rates of **2** for CV measurements.

Fig. S10. (a) CV curves of **1** at different scan rates. (b) Curves of the peak currents vs the square roots of scan rates of **1**. (c) GCD curves of **1** at different current intensities.
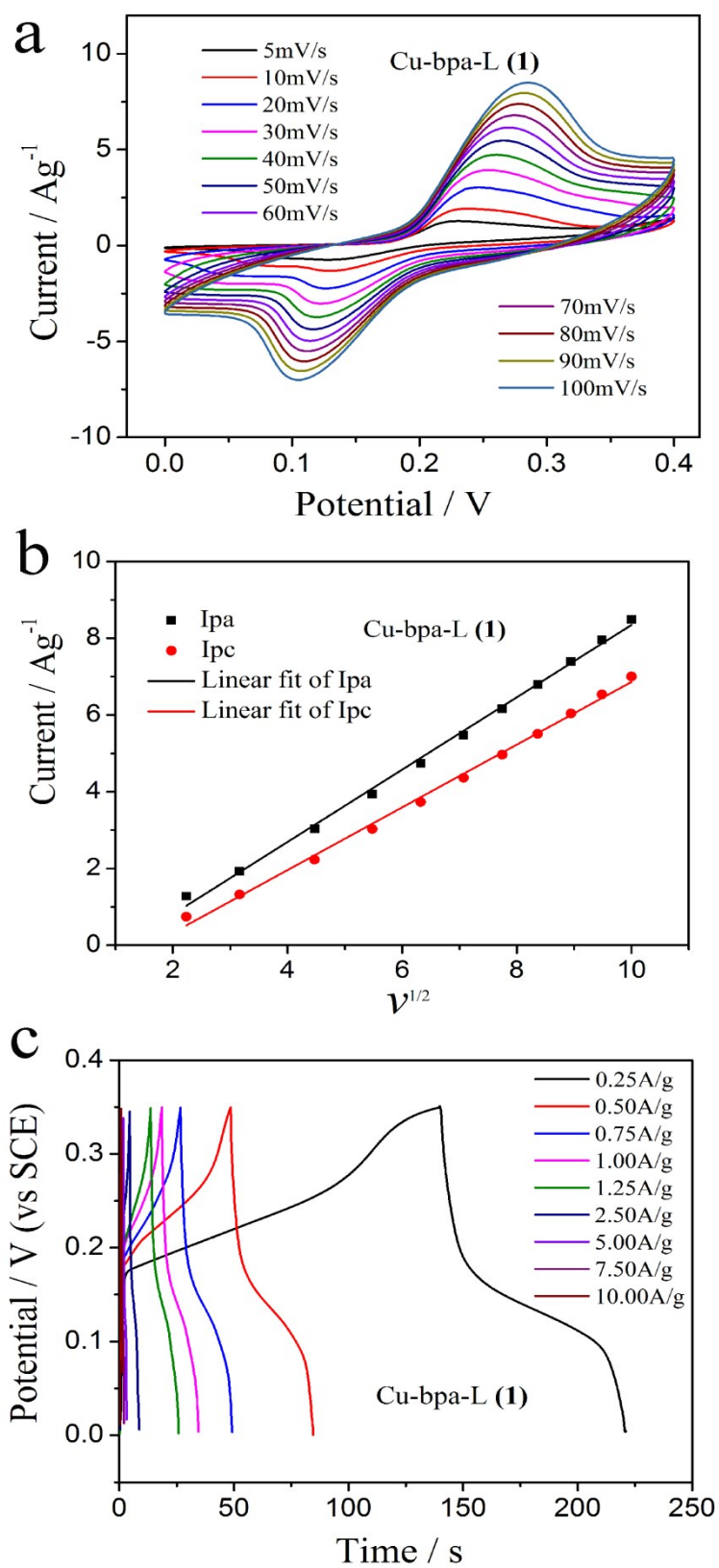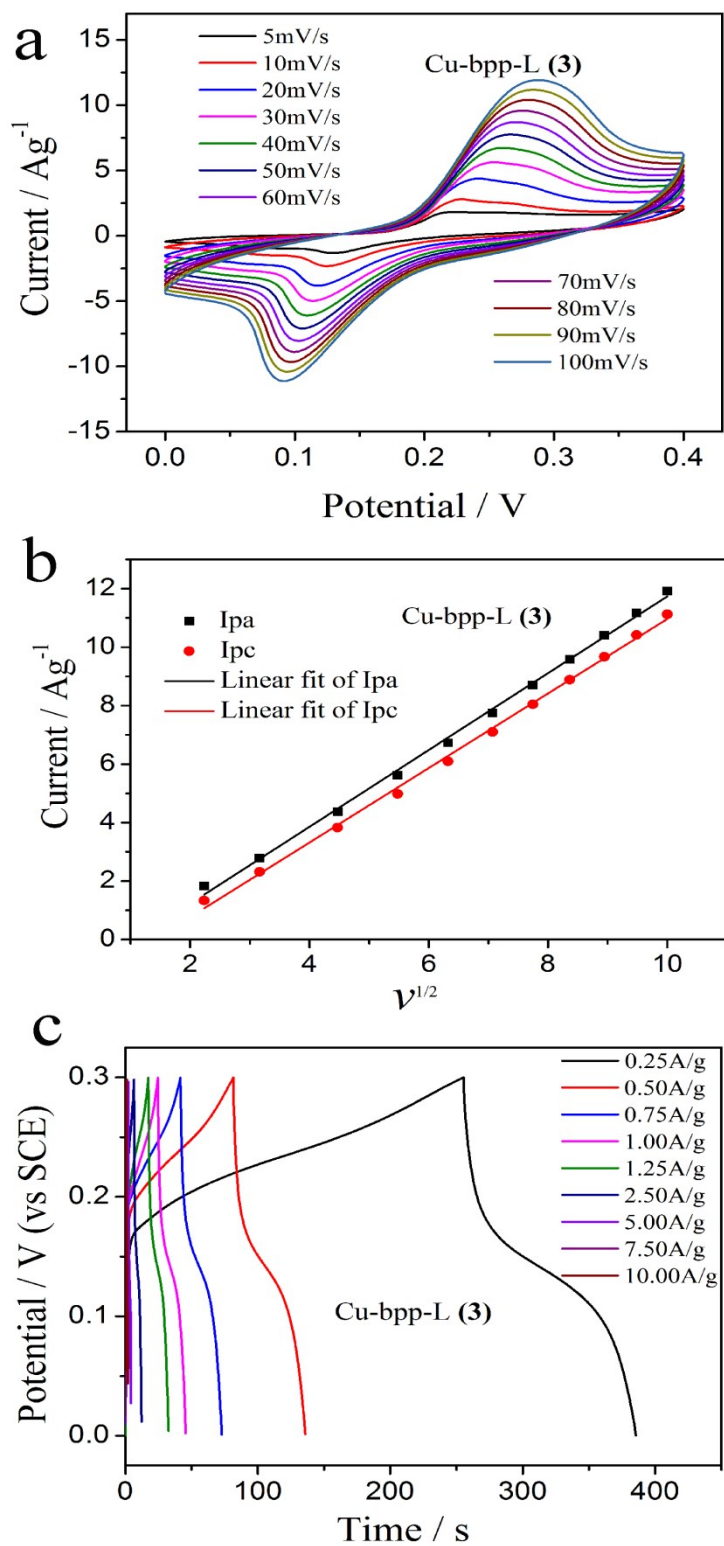
Fig. S11. (a) CV curves of **3** at different scan rates. (b) Curves of the peak currents vs the square roots of scan rates of **3**. (c) GCD curves of **3** at different current intensities.

3. TABLE

Table S1. Crystal data and structural refinement parameters for compounds **1–3**.

	Cu-bpa-L(1)	Cu-bpe-L(2)	Cu-bpp-L(3)
formula	$C_{44}H_{38}CuN_4O_8S_{12}$	$C_{45}H_{44}CuN_4O_{12}S_{12}$	$C_{46}H_{46}CuN_4O_{10}S_{12}$
fw	1199.04	1281.10	1263.20
cryst size (mm³)	0.15×0.18×0.38	0.10×0.15×0.30	0.10×0.15×0.32
cryst syst	monoclinic	monoclinic	monoclinic
space group	$C2/c$	$P2_1/n$	$P2_1$
a (Å)	24.0590(19)	8.4066(7)	9.1976(3)
b (Å)	9.0771(6)	26.390(2)	16.9404(6)
c (Å)	25.3307(18)	24.841(2)	17.7175(6)
α (deg)	90	90	90
β (deg)	112.705(4)	94.326(3)	95.852(1)
γ (deg)	90	90	90
V (Å³)	5103.2(7)	5495.4(8)	2746.20(16)
Z	4	4	2
ρ_{calcd} (g·cm⁻³)	1.550	1.548	1.525
$F(000)$	2428	2636	1277.8
μ (mm⁻¹)	0.974	0.915	0.894
T (K)	223(2)	223(2)	223(2)
reflns collected	35394	139857	104004
unique reflns	5820	12591	12626
observed reflns	3855	8701	12626
no. params	342	705	699
GOF on F^2	1.190	1.077	1.039
R_1 / R_1 [I>2σ(I)]	0.1029 / 0.0739	0.0929 / 0.0508	0.0485 / 0.0365
$_wR_2 / {_w}R_2$ [I>2σ(I)]	0.1715 / 0.2020	0.1109 / 0.1204	0.1001 / 0.1001

4. EQUATIONS

$$C_{sp} = \frac{\int_{V_0}^{V} I(V)\,dV}{mv(V - V_0)} \qquad (1)[5]$$

where C_{sp} (F g^{-1}), m (g), v (V s^{-1}), (V$^-$V$_0$), and I(V) are the specific capacitance, mass of the active material, potential scan rate, potential range and current density, respectively.

$$C'_{sp} = \frac{I \times \Delta t}{\Delta V \times m} \qquad (2)[5]$$

where C_{sp}' (F g^{-1}) is the discharge specific capacitance, I is the discharge current (A), Δt is the discharge time (s), ΔV is the potential window, and m is the mass (g) of the active material.

References

1. P. Hudhomme, S. L. Moustarder, C. Durand, N. Gallego-Planas, N. Mercier, P. Blanchard, E. Levillain, M. Allain, A. Gorgues and A. Riou, S-Position isomers of BEDT-TTF and EDT-TTF: Synthesis and influence of outer sulfur atoms on the electrochemical properties and crystallographic network of related organic metals. *Chem. Eur. J.*, 2001, **7**, 5070–5083.

2. R. D. McCullough, M. A. Petruska and J. A. Belot, Investigating the synthesis of unsymmetrical tetrathiafulvalene derivatives: Improved yields by the hidden equivalent method. Tetrahedron, 1999, **55**, 9979–9998.

3. G. M. Sheldrick, SHELXS-2016, Program for structure solution; Universität of Göttingen: Germany, 2016.

4. G. M. Sheldrick, SHELXL-2016, Program for structure refinement; Universität of Göttingen: Germany, 2016.

5. M. Lu, X.-P. Yuan, X.-H. Guana, and G.-S. Wang, Synthesis of nickel chalcogenide hollow spheres using an L-cysteine-assisted hydrothermal process for efficient supercapacitor electrodes. *J. Mater. Chem. A*, 2017, **5**, 3621–3627.